nature communications

Article

https://doi.org/10.1038/s41467-026-73939-8

Revealing bond level origin of stability in disordered solids from marginal stability to ultrastability

Received: 10 January 2025

Accepted: 21 May 2026

Published online: 31 May 2026

Check for updates

Junchao Huang [1], Jianhua Zhang [2], Ding Xu [2], Shiyun Zhang [2], Hua Tong [2] ✉ & Ning Xu [1,2,3] ✉

Disordered solids can be prepared with a vast spectrum of stabilities, ranging from marginally stable to ultra-stable. While understanding the structural origin of stability is crucial for predicting mechanical failure, as well as for revealing the nature and manipulating the properties of disordered solids, structural disorder poses a significant obstacle. Here, we propose and identify stabilizing bonds—interactions between particles whose removal would trigger mechanical failure—as a key microscopic feature governing stability. We present compelling evidence that stabilizing bonds dictate marginal stability, demonstrated by their recovery of the weak force distribution predicted by theories and their power to predict failure under load. The evolution from marginal stability to ultra-stability is further captured by the amount, spatial organization, and unstable modes of stabilizing bonds, revealing their role as 'defects' in disordered solids. Our work establishes stabilizing bonds as a fundamental structural entity responsible for unusual properties of disordered solids, paving the way for a generalized description of these materials.

Under fast cooling or compression, almost all liquids can form disordered solids[1–4]. Comprehending the formation and nature of these ubiquitous materials[5] remains a major challenge in physics and materials science, due to their disordered and nonequilibrium characteristics[3,4,6]. The difficulty stems not only from the lack of repeatable unit cells for mathematical analysis, as in crystals, but also from spatially heterogeneous structures and elastic responses. Therefore, the conventional wisdom from crystal physics—that mechanical instabilities are typically initiated by defects—cannot be simply applied to disordered solids. To characterize structural heterogeneity, numerous local measurements have been proposed, such as coarse-grained local shear stress or modulus[7–10], sterically favored structures[10,11], and soft spots[10,12–15]. Beyond particle-based analysis, recent studies reveal that bond-level microscopic perspectives[16] can unveil hidden features and guide mechanical metamaterial design[17–20].

Due to inherent disorder and heterogeneity, no two bonds in disordered solids contribute equally. Identifying each bond's precise role in maintaining stability is thus a critical issue. Recently, two distinct bond types were uncovered: stabilizing and non-stabilizing[21]. By definition, stabilizing bonds are crucial for preserving solid stability, as their removal triggers an unstable mode leading to mechanical failure. These ubiquitous bonds exhibit strong spatial correlations with soft spots across various potentials, suggesting a predictive capability for local particle rearrangements triggered by instabilities under load[21]. Here, we explore stabilizing bonds to reveal deeper physical insights across a spectrum of stabilities, from marginally stable to ultra-stable.

Apparently, the stability of a disordered solid is jointly determined by bond connectivity and the stress bonds bear. The Maxwell criterion[22] sets a lower limit on connectivity for mechanical stability: when the average coordination number z equals the isostatic value

[1]Hefei National Research Center for Physical Sciences at the Microscale, University of Science and Technology of China, Hefei, People's Republic of China. [2]Department of Physics, University of Science and Technology of China, Hefei, People's Republic of China. [3]College of Physics, Guizhou University, Guiyang, People's Republic of China. ✉e-mail: huatong@ustc.edu.cn; ningxu@ustc.edu.cn

$z_{iso} = 2D$ (D being the spatial dimension), connectivity is just sufficient to maintain stability. This isostaticity exemplifies marginal stability—a critical state between stable and unstable regimes[4,15,23–32]. Frictionless particle packings at the jamming transition are isostatic[4,24,33,34], serving as prototypes for understanding marginal stability[28,30–32]. Recent studies of isostatic hard-sphere packings suggest that marginal stability restricts the weak interparticle force distribution $P(f)$ to a power-law form, $P(f) \sim f^{\theta}$[4,25,26,28,30–32]. Full replica-symmetry-breaking theory predicts a mean-field exponent $\theta = 0.42311\cdots$ in infinite dimensions[4,25], while in finite dimensions, localized excitations yield an observed $\theta = 0.17462\cdots$[30–32,35].

Whether theories for isostatic packings generalize to hyperstatic systems ($z > z_{iso}$) remains unclear. Above the jamming transition, a delicate balance between bond connectivity and stress yields multiple critical scaling relations with respect to $\Delta z = z - z_{iso}$[4,23,24,32–34,36–40]. While hyperstatic packings might retain signatures of isostatic marginal stability[15,27,29,32], recent evidence shows that the $P(f)$ exponent θ varies with Δz[41–43]. This variability challenges the straightforward generalization of marginal stability to hyperstatic systems.

Disordered solids, such as structural glasses, are typically hyperstatic and resist external perturbations, with resistance increasing alongside glass stability. Generally, glasses become more stable when quenched at slower rates[1,3,44,45]; indeed, ultra-stable glasses—prototypes of ideal glasses—can now be fabricated in experiments[46] and simulations[47–50]. Regardless of stability, disordered solids undergo mechanical failure under load via elastic-plastic deformation[51–55]. On the verge of instability, the solids also exhibit marginal stability. This stress-induced marginal stability, however, is distinct from that arising from isostaticity at the jamming transition.

Despite separate studies on isostaticity- and stress-induced marginal stability and on glasses with varying stability, a fundamental question remains: can all these stability-related phenomena be universally described within a single framework?

Through the study of jammed packings across various pressures, glasses with stability ranging from marginal to ultra-stable, and glasses approaching shear-induced instabilities, we provide compelling evidence that stabilizing bonds form the foundation for a unified framework. For jammed packings, the fraction of stabilizing bonds decreases with increasing pressure p and reaches a minimum at a crossover pressure p_c, signaling a change from isostaticity-dominant to stress-dominant nature. The exponent θ of the weak force distribution for these bonds agrees with theoretical values, suggesting their role in supporting marginal stability. In glasses under shear, the fraction of stabilizing bonds increases remarkably near instability, where opening a single bond excites the soft mode responsible for failure. For glasses with varying stability, both the fraction and cluster size of stabilizing bonds decrease as stability increases. While clustering in less stable ordinary glasses, stabilizing bonds become rare, mostly isolated, or even disappear in ultra-stable glasses. These results indicate that stabilizing bonds act as 'defects' in disordered solids. Their population and spatial distribution thus naturally determine overall stability, leading to a unified description of the phenomena studied here. We expect that this framework will enable a deeper understanding of the unusual properties of disordered solids across the entire stability spectrum.

Results

The first four of six subsections focus on marginal stability in hyperstatic packings with harmonic potential ($\alpha = 2$ in Eq. (3); see "Methods"). For generality, results for Hertzian ($\alpha = 5/2$) and $\alpha = 3$ potentials are provided in the Supplementary Information (SI). The final two subsections discuss marginal stability upon approaching shear instability and evolution with varying stability in inverse-power-law (IPL) glasses (see "Methods").

Fraction of stabilizing bonds

We construct a force network by connecting interacting particle pairs with bonds. To identify stabilizing bonds, we remove a bond while keeping the rest of the network unchanged and update the Hessian matrix. If the updated Hessian possesses a negative eigenvalue, the bond is stabilizing, as its absence triggers an unstable mode leading to mechanical failure[21]. Otherwise, the bond is classified as non-stabilizing[21].

Figure 1a, b illustrates the pressure p and system sizes N dependence of the fraction of stabilizing bonds, denoted as η, in two- and three-dimensional (2D and 3D) jammed solids, respectively. In the $p \to 0$ limit at the jamming transition, isostaticity dictates that removing any single bond causes mechanical failure. Consequently, all bonds are stabilizing ($\eta = 1$), as precisely demonstrated in Fig. 1a, b. When pressure increases, more bonds form and the force network becomes hyperstatic. While increasing pressure tends to destabilize the solid, the additional bonds provide stabilization. The competition and delicate balance between these two factors result in a continuous decrease in η with p. This trend reverses at a nearly N-independent crossover pressure $p_c \approx 0.04 \pm 0.01$, beyond which η rises. The p_c value exhibits only a weak dependence on spatial dimension.

As observed in Fig. 1a, b, the $\eta = 1$ plateau at low pressure persists to a pressure that decreases with increasing system size. Prior studies indicate that finite-size effects extend isostaticity to a pressure proportional to $N^{-2(\alpha-1)}$[38,39]. Thus, the $\eta \approx 1$ plateau likely stems from the same effect. This is confirmed in Fig. 1c, d, where low-pressure data for different system sizes show excellent scaling collapse when η is plotted against $pN^{2(\alpha-1)}$ (pN^2 for harmonic potential). This collapse suggests that the behavior of stabilizing bonds near the jamming transition is controlled by isostaticity, manifesting typical jamming criticality. This is further supported by the behavior of particle clusters connected via stabilizing bonds. As shown in Fig. S9 of the SI, the size of the largest such cluster scales with Δz. Moreover, at a given $\Delta z > 0$, the size grows with system size, tending to diverge in the $N \to \infty$ limit. This suggests an unusual nature of packings near jamming, distinct from conventional critical phenomena.

While the crossover pressure p_c appears insensitive to system size, the minimum η value, η_{min}, gradually decreases as N increases. As shown in Fig. 1e, f, $\eta_{min} - \eta_\infty$ follows a power-law scaling with the system size N:

$$\eta_{min} - \eta_\infty \sim N^{-w}, \tag{1}$$

where $(\eta_\infty, w) \approx (0.081, 1.211)$ in 2D and $(0.031, 0.703)$ in 3D. The fitting parameter η_∞ represents the asymptotic minimum fraction of stabilizing bonds as $N \to \infty$. This suggests that, even in the large-system-size limit, jammed solids quenched instantaneously from random states retain a non-zero fraction of stabilizing bonds. We will show later that this is a characteristic of ordinary glasses quenched from high temperatures; in contrast, stabilizing bonds can be entirely absent in finite-size ultra-stable glasses.

The non-monotonic pressure dependence of η is particularly intriguing and unusual in jamming physics. Since stabilizing bonds indicate mechanical stability, the presence of a minimal η suggests a change in the underlying mechanism across p_c. In the following, we will characterize the change from multiple aspects.

Weak force distribution

Isostaticity leads to marginal stability. A hallmark of this isostatic marginal stability is the power-law distribution of the weak force $P(f)$. As aforementioned, the exponent θ of $P(f)$ is found to change with pressure in jammed packings[41–43]. Since bonds bear forces, it is natural to explore the possible link between variations of $\theta(p)$ and $\eta(p)$. What roles do stabilizing bonds play, particularly across p_c?

https://doi.org/10.1038/s41467-026-73939-8

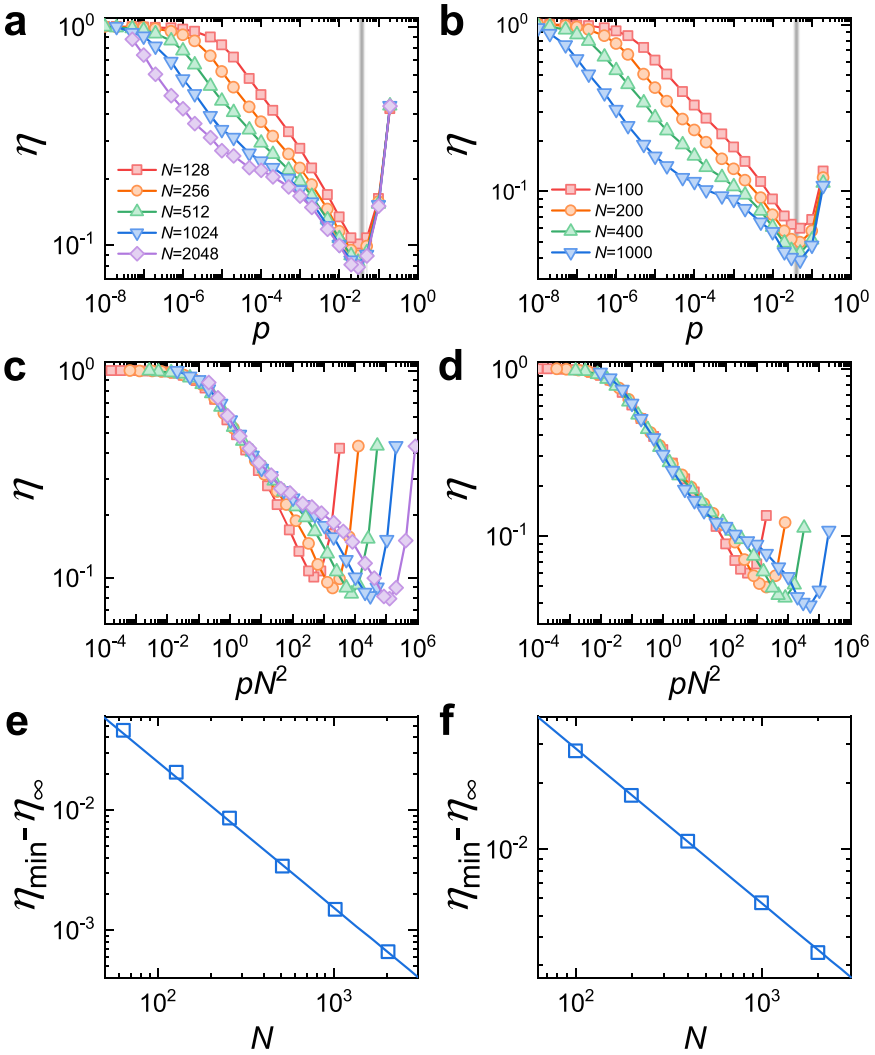

Fig. 1 | Non-monotonic pressure dependence of the fraction of stabilizing bonds. The left and right panels are for 2D and 3D systems, respectively. **a**, **b** Fraction of stabilizing bonds η as a function of pressure p for different system sizes. The vertical gray bands mark the crossover around $p_c \approx 0.04 \pm 0.01$ where η reaches the minimum value $\eta_{\min}$. **c**, **d** Scaling collapse of the low-pressure parts of all $\eta(p)$ curves shown in (**a**) and (**b**) when η is plotted against pN^2. **e**, **f** System size evolution of the minimal value $\eta_{\min}$. Here η_∞ is an extrapolation of $\eta_{\min}$ in the $N \to \infty$ limit, which are 0.081 and 0.031 for 2D and 3D, respectively. The solid lines are power-law fits, which have a slope of -1.211 (**e**) and -0.703 (**f**), respectively. Source data are provided as a Source Data file.

Figure 2a, d shows cumulative force distributions for all bonds, denoted as $G(f)$, for $N = 1024$ and 1000 systems in 2D and 3D, respectively. Consistent with previous studies[35,41], we use cumulative force distributions to suppress statistical noise in the weak-force tail, thereby enabling a more robust and clear extraction of the underlying asymptotic behavior of $P(f)$. The distributions exhibit a power-law scaling behavior in the weak force regime: $G(f) \sim f^{1+\theta}$. The exponent θ decreases with increasing pressure, from approximately 0.17 at $p \to 0$ to almost zero near p_c, inconsistent with theoretical predictions for isostatic marginal stability. To resolve this, we calculate the weak force distributions for stabilizing and non-stabilizing bonds, $G_s(f)$ and $G_n(f)$, separately. The total distribution is then:

$$G(f) = \eta G_s(f) + (1-\eta) G_n(f). \tag{2}$$

Taking $p = 10^{-4}$ as an example, Fig. 2b, e compares $G_s(f)$, $G_n(f)$, and $G(f)$ in 2D and 3D, respectively. Both $G_s(f)$ and $G_n(f)$ exhibit power-law scaling: $G_s(f) \sim f^{1+\theta_s}$ and $G_n(f) \sim f^{1+\theta_n}$, where $\theta_s \approx 0.17$ differs from $\theta_n \approx 0.02$. As seen from Fig. 1, the fraction η is small at $p = 10^{-4}$ (0.24 in 2D and 0.11 in 3D). Consequently, according to Eq. (2), the exponent θ for all bonds is biased towards θ_n due to the dominance of non-stabilizing bonds.

Figure 2c, f shows pressure evolution of θ, θ_s, and θ_n in 2D and 3D, respectively. These values are also confirmed by the system-size scaling of the minimal force, demonstrated in Fig. S11 of the SI. Interestingly, when $p < p_c$, θ_s remains 0.17, matching the theoretical value for isostatic marginal stability in finite dimensions[30–32]. In contrast, θ_n decreases with increasing pressure and fluctuates around zero at high pressures. Because η decreases with increasing p until $p = p_c$, we can thus conclude from Eq. (2) that the decrease in θ away from the jamming transition is primarily contributed by $\theta_n(p)$.

At isostaticity, removing any weak force bond would destabilize a hard-particle packing, resulting in $\theta \approx 0.17$ in finite dimensions[28,30,31,35]. In hyperstatic systems, this destabilizing effect is specifically triggered by removing a stabilizing bond rather than a non-stabilizing one. Therefore, above jamming, it is the stabilizing bonds that bear weak forces and are responsible for marginal stability when $p < p_c$, conforming to the theoretical requirement of isostatic marginal stability. The observation that $\theta_s \approx 0.17$ strongly supports this scenario, generalizing the applicability of marginal stability theories to hyperstatic

systems. Given that stabilizing bonds are responsible for marginal stability, the observed growth of the largest clusters they form (Fig. S9 of the SI) implies that jammed packings are marginally stable in the large-N limit at low pressures.

Another aspect of weak force distributions in isostatic hard-particle packings in low dimensions is that buckler particles with $D+1$ bonds are inevitable. These localized excitations contribute an exponent $\theta_l = 0.17462\cdots$, while extended excitations from other particles yield $\theta_e = 0.42311\cdots$, as predicted by mean-field theories[35]. Following Ref. 35, we identify bucklers and divide stabilizing bonds into these two classes. As depicted in Fig. 3, for both 2D and 3D, the exponent for stabilizing bonds connected to bucklers remains approximately 0.17 when $p < p_c$, whereas other stabilizing bonds contribute an exponent of approximately 0.40, consistent with the picture of Ref. 35.

To further verify whether the identified stabilizing bonds remain relevant to marginal stability independently of localized buckling excitations, we perform an additional sub-network analysis. As shown in Figs. S16 and S17 of the SI, even after bonds contributed by all operationally defined localized bucklers are excluded, the remaining extended network still requires the stabilizing-bond criterion to recover the universal marginal scaling (the theoretically predicted weak force distribution). Moreover, the fraction of these stabilizing bonds relative to the remaining contacts varies with pressure in a manner consistent with Fig. 1. Together, these results support the interpretation that stabilizing bonds form the relevant backbone of marginal stability in hyperstatic systems, regardless of bucklers.

Figure 2c, f also shows that θ_s rapidly increases beyond p_c, eventually saturating at the theoretical value of 0.42 in both 2D and 3D. Notably, in this high-pressure regime, the coordination number significantly exceeds the isostatic value, and no existing theory confirms if 0.42 retains its original significance. Consequently, the meaning of this plateau remains unclear. However, Fig. 1 shows that η grows rapidly when $p > p_c$, making stabilizing bonds dominant once again, similar to the condition near the jamming transition. Whether a hidden transition plays a role in this high-pressure marginal stability requires further investigation. As marked in Fig. 2c, f, the transition from marginal to deep jamming corresponding to $z = 6$ in 2D and $z = 12$ in 3D[40] is a possible candidate responsible for this behavior, as discussed in Fig. S6 of the SI.

Crossover from isostaticity-dominant to stress-dominant

The minimum of η (Fig. 1a, b) and the remarkable deviation of θ_s from 0.17 (Fig. 2c, f) imply some change in the nature of stabilizing bonds across p_c. As aforementioned, increasing coordination number and internal stress have opposing effects on the stability of jammed solids[15,29,32,56]. The fraction of stabilizing bonds arises from the competition and delicate balance between these two factors. Note that in unstressed hyperstatic networks, stabilizing bonds do not exist; thus, they are only meaningful when internal stress is nonzero. Consequently, decomposing the contributions of these two factors would be essential for understanding the non-monotonic behavior of $\eta(p)$ and the change in the nature of stabilizing bonds at p_c.

To estimate the contribution of coordination number, we connect the two closest non-interacting particles in a jammed solid with an unstressed harmonic spring. Adding this extra bond enhances stability while keeping internal stress constant. Consequently, it is expected

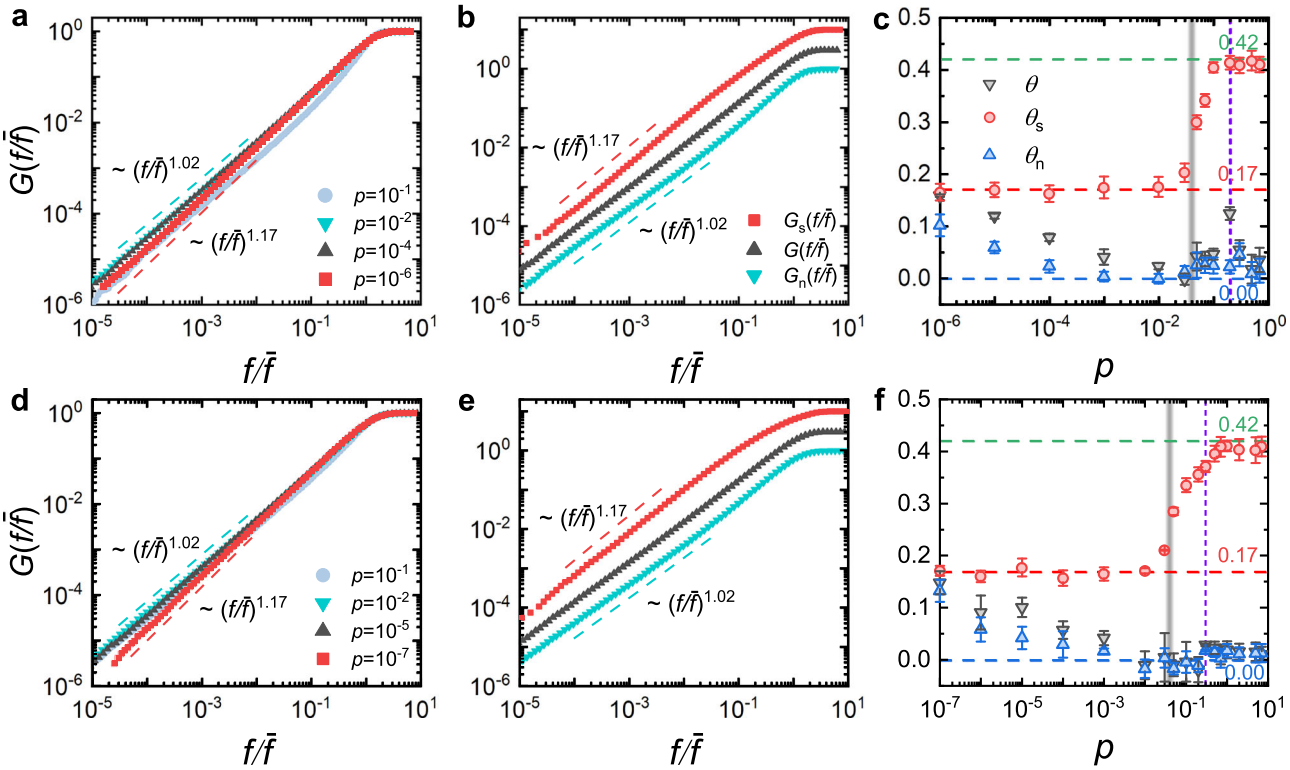

Fig. 2 | Pressure evolution of the weak force distribution. Upper and lower panels represent $N = 1024$ and 1000 systems in 2D and 3D, respectively. **a**, **d** Cumulative force distribution for all bonds, $G(f/\bar{f})$, at various pressures, where $\bar{f}$ is the average force. Red and cyan dashed lines show the approximate $G(f) \sim f^{1.17}$ and $G(f) \sim f^{1.02}$ behaviors for weak forces at $p = 10^{-6}$ and 10^{-2} in 2D and at $p = 10^{-7}$ and 10^{-2} in 3D. **b**, **e** Comparison of $G(f)$, $G_n(f)$ (non-stabilizing), and $G_s(f)$ (stabilizing) at $p = 10^{-4}$. For each curve, $\bar{f}$ is the average force of the respective bond type. Curves are vertically shifted for clarity. Red and cyan dashed lines show the approximate $G_s(f) \sim f^{1.17}$ and $G_n(f) \sim f^{1.02}$ behaviors for weak forces. **c**, **f** Pressure dependence of the weak force distribution exponents θ, θ_n, and θ_s for $G(f)$, $G_n(f)$, and $G_s(f)$, respectively. The vertical gray band marks the crossover near p_c, and purple dashed lines indicate the marginal-to-deep jamming transition. From top to bottom, the horizontal dashed lines mark the values of 0.42, 0.17, and 0, respectively. Error bars in (**c**, **f**) represent the standard deviation of the fitted exponents, determined by varying the fitting intervals across pooled data from multiple configurations. Source data are provided as a Source Data file.

https://doi.org/10.1038/s41467-026-73939-8

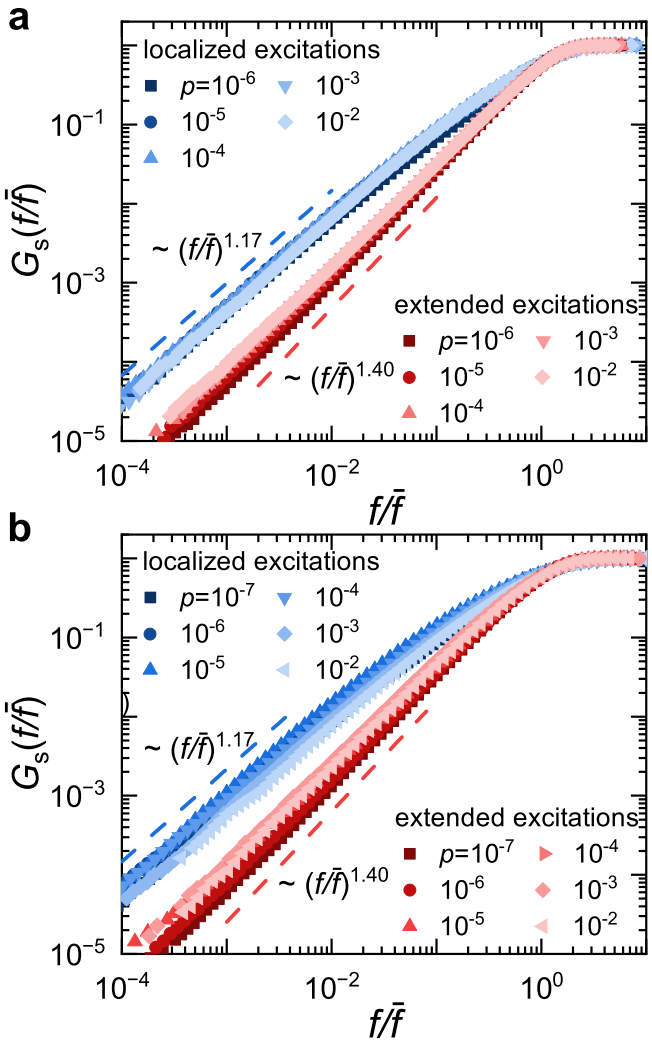

Fig. 3 | Classification of localized and extended contributions to the weak force distribution of stabilizing bonds below p_c. a Cumulative force distributions $G_s(f)$ due to localized (blue) and extended (red) excitations for $N = 1024$ systems in 2D. **b** Results for $N = 1000$ systems in 3D. The blue and red dashed lines show the approximate $G_s(f) \sim f^{1.17}$ and $G_s(f) \sim f^{1.40}$ behaviors for bucklers and the others, respectively. Source data are provided as a Source Data file.

that the change in η due to this addition, denoted as $\Delta\eta_z$, would be negative, as confirmed by Fig. 4a. Near isostaticity ($p \to 0$), adding an unstressed bond greatly enhances stability, making $|\Delta\eta_z|$ largest. As pressure and coordination number z increase, the influence of an additional bond typically lessens, decreasing $|\Delta\eta_z|$. One might expect this trend to continue at high pressures. However, Fig. 4a presents a counter-intuitive result: $|\Delta\eta_z|$ reaches a minimum at $p \approx p_c$, and then begins to increase with further increasing pressure. This indicates that adding a bond starts to affect the stability more significantly again beyond p_c. This non-monotonic behavior of $\Delta\eta_z(p)$ has to be induced by a significant change in the influence of internal stress across p_c.

To investigate the contribution of internal stress, we multiply the internal stress by a factor δ (defined in Methods) while keeping the force network configuration unchanged. This procedure preserves mechanical balance. Decreasing (increasing) δ from unity stabilizes (destabilizes) the solid, thereby decreasing (increasing) η. Logically, if stabilizing bonds are primarily controlled by internal stress, the variation of η would be sensitive to the change in δ. We denote the change in η from $\delta = 1$ to $\delta = 0.99$ as $\Delta\eta_\sigma$, which is negative, and show its pressure dependence in Fig. 4a. At pressures up to p_c, $\Delta\eta_\sigma(p)$ decreases mildly, indicating that internal stress plays a comparable role in destabilizing solids in this regime. Interestingly, above p_c, $|\Delta\eta_\sigma|$ increases rapidly, suggesting that internal stress becomes the dominant factor controlling stabilizing bonds when $p > p_c$.

The above analysis suggests that the minimum fraction η_{min} at $p = p_c$ reveals a hidden crossover from a low-pressure regime predominated by coordination number to a high-pressure regime predominated by stress. The most peculiar feature of marginally jammed solids above the jamming transition is that their properties are strongly controlled by isostaticity, as measured by the excess coordination number $\Delta z = z - z_{iso}$. It is thus plausible to name the $p < p_c$ regime as isostaticity-dominant. Therefore, we conclude that the nature of stabilizing bonds, and hence marginal stability changes from isostaticity-dominant to stress-dominant across p_c.

Besides the changing nature of stabilizing bonds, the rapid growth of θ_s across p_c suggests that bucklers—contributing to $\theta_s \approx 0.17$—become rare or disappear. While expected at high pressures, it is unclear if this occurs near p_c. We address this by tracking the fraction of particles with three bonds (f_3), which accounts for all bucklers. As shown in Fig. 4b, f_3 diminishes with pressure, reaching zero above p_c, as visualized in 2D configurations (Fig. 4c–e). The disappearance of bucklers above p_c eliminates a channel for localized excitations, consistent with θ_s approaching the mean-field value for collective excitations. However, further studies are needed to confirm if this value remains applicable at such high pressures. Compared to marginal stability near jamming, the stress-dominant regime is largely unexplored; our findings necessitate new theories focused on stress-dominant marginal stability.

Due to their localized rather than extended excitations, bucklers play a less dominant role than other particles in determining macroscopic properties. Consequently, while inevitable at low pressures and in low dimensions, bucklers are not key elements for the overall stability, elasticity, or jamming scalings[30].

Deviation of jamming scalings

Due to the jamming criticality and isostaticity, multiple scaling relations exist in marginally jammed solids[4,23,24,32–34,36–39,57,58]. Since p_c marks the crossover from isostaticity-dominant to stress-dominant, it can be expected that the scaling relations stemming from isostaticity would deviate for $p > p_c$. This is precisely confirmed by detailed analyses. Figure 5a, b demonstrates that typical scaling relations of the excess coordination number, $\Delta z \sim p^{1/2}$, and the shear moduli, $G \sim p^{1/2}$, persist up to p_c for harmonic potential for varying system sizes in both 2D and 3D, respectively. Significant deviations occur when $p > p_c$.

We further consider the scaling behavior related to mechanical instabilities. Recently, the response of marginally jammed solids to external loads has shown unusual scaling relations[21,51–54,59,60]. Specifically, the yield stress σ_y associated with incipient instabilities under shear displays robust scaling relations with system size and pressure: $\sigma_y \sim N^{-0.65}p^{1.08}$ [54]. In Fig. 5c, we present $\sigma_y(p)$ across p_c for various system sizes in 2D and 3D. When plotting $\sigma_y N^{0.65}$ against p, all curves collapse nicely. Again, the scaling $\sigma_y \sim N^{-0.65}p^{1.08}$ holds only for $p < p_c$, with significant deviations occurring for $p > p_c$.

Therefore, jamming scalings terminate near p_c, marking the departure from isostaticity-based physics at high pressures. While previous studies attributed this breakdown to elastic instabilities[29], our observed mechanism is fundamentally different. The breakdown occurs when η reaches its minimum—a point where packings are actually more stable than those at lower pressures, where scalings still hold. The breakdown is therefore not a result of diminishing stability, but a natural consequence of key findings discussed above. In short, beyond merely noting the breakdown, our work reveals a novel, stability-based underlying mechanism for it, explaining both where and why they fail.

Marginal stability under shear

Ordinary glasses are typically hyperstatic and resistant to external loads. Subjecting them to sufficient compression or shear induces mechanical failure, leading to a new state of stress-induced marginal stability via elastic-plastic deformation. Since stabilizing bonds encode features of marginal stability, this raises the question of whether they can also serve as markers for this stress-induced marginal stability.

To address this question more generally, we present results here for 2D IPL glasses under quasistatic shear. We have verified that our results are robust against system size and spatial dimensionality (see Fig. S13 of the SI). Figure 6a shows the stress-strain ($\sigma - \gamma$) relations for an ordinary and an ultra-stable glass with $N = 256$ particles, quenched from high and low parent temperatures T_p, respectively (see "Methods"). Under quasistatic shear, both glasses undergo successive elastic-plastic processes, marked by linear stress increases and discontinuous drops. We focus on the incipient instability. Due to their distinct stability, the ultra-stable and ordinary glasses exhibit brittle and ductile behaviors, respectively[61,62]. Consequently, the incipient critical shear stress σ_c and strain γ_c are significantly larger for the ultra-stable glass than for the ordinary glass.

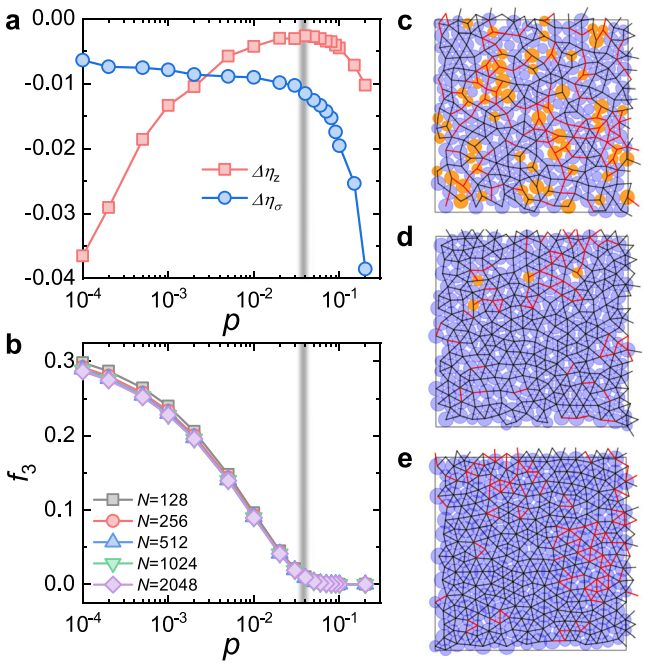

Fig. 4 | Evidence of the change in the nature of stabilizing bonds across p_c. **a** Pressure dependence of the changes in the fraction of stabilizing bonds due to the addition of an unstressed bond, $\Delta\eta_z$, and a slight decrease of internal stress (by multiplying $\delta = 0.99$ to the internal stress), $\Delta\eta_\sigma$, for $N = 1024$ systems in 2D. **b** Pressure dependence of the fraction of particles with three bonds, $f_3(p)$, for systems with different sizes in 2D. **c**–**e** Configurations of jammed solids comprising $N = 256$ particles, with force networks for $p = 0.001$, 0.03, and 0.1, respectively. Stabilizing and non-stabilizing bonds are in red and black, respectively. Particles with three bonds are highlighted in orange. Note that there are no bucklers in (**e**). The vertical gray band in (**a**, **b**) marks the crossover around p_c. Source data are provided as a Source Data file.

Figure 6b demonstrates that, as the instability is approached ($\delta\sigma = \sigma_c - \sigma \to 0$), the lowest normal-mode frequency ω_L for both glasses scales as $(\delta\sigma)^{1/4}$. This scaling is consistent with fold-instability theory[54] and signals the development of a soft mode. The emergence of a soft mode, which is also a hallmark of the jamming transition, establishes a common feature between these two distinct types of marginal stability.

As shown in Fig. 1, the fraction of stabilizing bonds η increases as the jamming transition is approached. Figure 6c shows a similar trend: η increases dramatically upon approaching the shear instability. Before shear is applied, $\eta = 0$ for the ultra-stable glass and 0.15 for the ordinary glass. They both reach over 0.85 at the smallest $\delta\sigma$ accessed here. At the current data precision, we cannot exclude the possibility that $\eta = 1$ when $\delta\sigma = 0$.

As directly visualized in Fig. S10 of the SI (see also the discussion in its caption), the rapid proliferation of stabilizing bonds on approaching the shear instability forms a pervasive, uniform network. This network provides a clear microscopic signature of the emergent marginal stability and establishes the precise condition that validates mean-field theories. Crucially, this structural evolution in stabilizing bonds and the insight it provides are inaccessible through the structures of soft modes and soft spots alone, which remain essentially unchanged with $\delta\sigma$.

The defining feature of a stabilizing bond is that removing it triggers an unstable mode **e** with a negative eigenvalue λ (decay time $\tau = (-i\sqrt{\lambda})^{-1}$). At jamming, opening a stabilizing bond excites the soft mode[28,30–32]. Since a soft mode also develops under shear, can this mode be excited when opening a stabilizing bond?

Intuitively, the stabilizing bond with the largest τ value – that is, the slowest unstable mode – is most crucial to stability. Opening it is thus most likely to trigger the soft mode responsible for the instability. We denote τ and **e** of such a bond as τ_s and $\mathbf{e}_s$, and calculate its projection onto the soft mode $\mathbf{e}_L$: $P_{ee} = \mathbf{e}_s \cdot \mathbf{e}_L / |\mathbf{e}_s||\mathbf{e}_L|$. Figure 6d shows that $P_{ee} = 1$ as the instability is approached in both glasses. Therefore, close to the instability, opening the stabilizing bond indeed triggers the soft mode. This behavior directly links stress-induced and isostaticity-induced marginal stabilities. We also find that as $\delta\sigma$ decreases, the number of stabilizing bonds whose unstable modes align with the soft mode increases.

Overall, information from stabilizing bonds—such as η (and its spatial distribution) and P_{ee}—signals the occurrence of instabilities under load. Although stress-induced and isostaticity-induced marginal

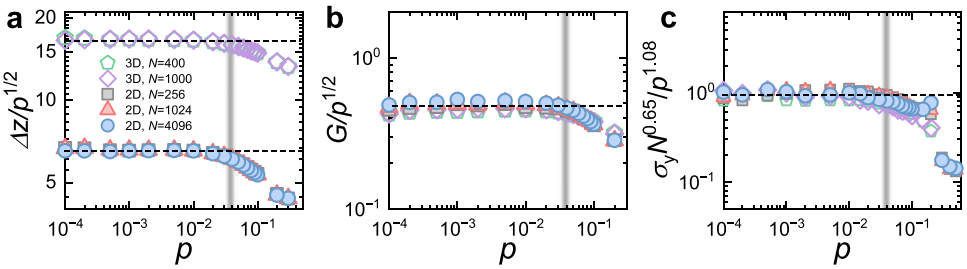

Fig. 5 | Deviation of jamming scalings above p_c. Pressure and system size dependence of **a** the excess coordination number Δz, **b** the shear modului G, and **c** the yield stress σ_y associated with the incipient shear instabilities for 2D (solid symbols) and 3D (empty symbols) systems. The horizontal dashed lines show jamming scalings $\Delta z \sim p^{1/2}$ in (**a**), $G \sim p^{1/2}$ in (**b**), and $\sigma_y \sim p^{1.08} N^{-0.65}$ in (**c**), respectively. The vertical gray bands mark the crossover regime around p_c. Source data are provided as a Source Data file.

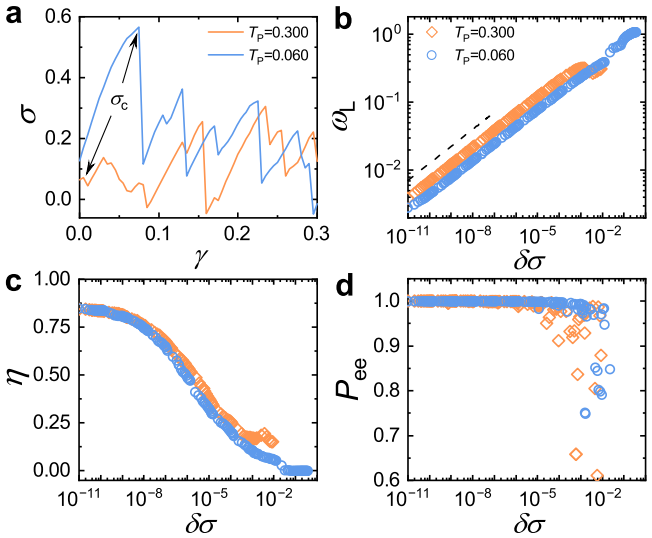

Fig. 6 | Signatures of marginal stability under shear in 2D IPL glasses with $N = 256$ particles. a Stress–strain ($\sigma - \gamma$) curves for two typical glass samples quenched from parent temperatures $T_p = 0.300$ (orange) and 0.060 (blue), corresponding to ordinary and ultra-stable glasses with ductile and brittle behaviors, respectively. Arrows indicate the incipient instability at the critical shear stress σ_c for both glasses. **b** Variation of the frequency of the lowest normal mode of vibration, ω_L, with the distance to instability $\delta\sigma = \sigma_c - \sigma$. The mode softens following the scaling, $\omega_L \sim (\delta\sigma)^{1/4}$ (dashed line), as predicted by the fold instability theory. **c** Variation of the fraction of stabilizing bonds η with $\delta\sigma$. **d** Variation of the projection P_{ee} (of the unstable mode with the longest decay time – triggered by breaking a stabilizing bond – onto the lowest normal mode of vibration) with $\delta\sigma$. P_{ee} approaches unity near the instability, acting as a precursor to the mechanical failure. Source data are provided as a Source Data file.

stabilities arise from different mechanisms and have been studied separately, our results suggest that they may be unified within the common framework of stabilizing bonds.

A broad spectrum of stability

Having highlighted the crucial role of stabilizing bonds in marginal stability, we now demonstrate their power in characterizing the full stability spectrum, particularly in ultra-stable glasses.

Instantaneously quenching an equilibrated liquid (at a parent temperature T_p lower than the onset temperature T_{on}) to zero temperature results in a glass (inherent structure) whose stability increases with decreasing T_p[1,3,44,45]. This trend is consistent with the energy-landscape-mediated dynamics below T_{on}[1]. For T_p below the mode-coupling temperature T_{mc} or the Vogel-Fulcher-Tammann temperature $T_{V\,FT}$, ultra-stable glasses are accessible using swap Monte-Carlo algorithms[63,64]. The IPL model efficiently generates these states, enabling us to span the full range from marginally stable to ultra-stable.

Figure 7 presents results for 2D IPL systems with $N = 256$ particles. The robustness of these results with respect to system size and spatial dimensionality is confirmed in Figs. S14 and S15 of the SI. Figure 7a shows the average potential energy of the inherent structures, U_{IS}, as a function of T_p. U_{IS} decreases monotonically as T_p is lowered, indicating an increase in glass stability. The decrease exhibits a crossover within the range between T_{mc} and $T_{V\,FT}$, transitioning from a slower rate at high T_p to a faster rate at low T_p.

Breaking a stabilizing bond is destructive to the overall stability of a disordered solid. Therefore, the more there are, the worse the stability is. This has been illustrated by the significant increase in η upon approaching both isostaticity-induced and stress-induced marginal stability. It is thus expected that η conversely decreases upon approaching ultra-stability, which is confirmed by Fig. 7b. The ensemble-averaged η decreases gradually for $T_p > T_{mc}$ and drops rapidly below $T_{V\,FT}$. In the limit of high stability, stabilizing bonds become extremely rare events. For the finite systems studied here ($N = 256$), we observe a fraction of states, $f_{\eta=0}$, where stabilizing bonds are entirely absent. As shown in Fig. 7b, $f_{\eta=0}$ increases as T_p decreases below T_{mc}, approaching unity in the $T_p \to 0$ limit. While the specific value of $f_{\eta=0}$ is subject to finite-size effects (as larger systems are statistically more likely to contain at least one rare stabilizing bond, see Fig. S14c of the SI), the physical trend of stabilizing bonds becoming sparse is universal.

Next, we analyze states that possess stabilizing bonds to further illustrate their properties. Figure 7c shows the T_p dependence of the decay time τ_s of the slowest unstable mode (defined above). Below T_{on}, τ_s decreases rapidly and tends to saturate at a lower limit in the ultra-stable regime. This decrease in τ_s coincides with a structural localization, as shown by the monotonic decrease in the participation ratio (PR) on the right axis of Fig. 7c. Together, these observations confirm a fundamental transition: in the ordinary glass regime (high T_p), stabilizing bonds trigger collective, slow modes; in the ultra-stable regime (low T_p), they trigger highly localized rearrangements with fast decay times.

Figure 7d, e shows the T_p dependence of the number of particle clusters connected via stabilizing bonds, n_s, and their maximum size, s_m. Both quantities decrease monotonically with decreasing T_p and saturate to a minimum below $T_{V\,FT}$. To directly visualize the evolution of the spatial distribution of stabilizing bonds with T_p, we show in Fig. 7f–i configurations in which stabilizing bonds and particles connected to them are highlighted. From left to right, T_p decreases across the four regions separated by T_{on}, T_{mc}, and $T_{V\,FT}$, respectively. As T_p decreases, the number of stabilizing bonds, the number of clusters, and the cluster sizes all decrease. In the ultra-stable regime, n_s and s_m saturate to 1 and 2, respectively, as visualized in Fig. 7i, suggesting that there is only one stabilizing bond connecting two particles.

The evolution of stabilizing bonds with glass stability suggests that they act as 'defects' in disordered solids. Ultra-stable glasses are defect-free or contain isolated defects. As stability weakens, these defects proliferate and aggregate, distinguishing ordinary glasses from ultra-stable ones. Thus, stabilizing bonds not only characterize marginal stability but also provide a unified metric for structural heterogeneity across the entire stability spectrum.

Discussion

In this work, we unveil the microscopic, bond-level origin of stability in disordered solids across the entire stability spectrum through the lens of stabilizing bonds. As physical carriers of marginal stability—typically represented by the weak force distribution—stabilizing bonds generalize the theory of marginal stability from isostatic to hyperstatic systems. We establish a link between marginal stability arising from isostaticity and that from mechanical failure under load by demonstrating their common features, such as the significant increase in the number of stabilizing bonds upon approaching them and the excitation of the soft mode via the breaking of a stabilizing bond. More generally, stabilizing bonds characterize the evolution from marginally stable to ultra-stable through their population, spatial organization, and the properties of their associated unstable modes. Our results position stabilizing bonds as fundamental defects in disordered solids, thereby providing a unified framework for characterizing and understanding the properties of these materials.

Stabilizing bonds, unlike soft spots, which are derived directly from vibrational modes and reflect quasilocalized modes (QLMs), are defined independently of such modes. However, they still exhibit strong spatial correlation with soft spots[21]. Moreover, both the number of stabilizing bonds and QLMs decrease with increasing stability and are strongly suppressed in ultra-stable glasses (Fig. 7 and Fig. S12 of

https://doi.org/10.1038/s41467-026-73939-8

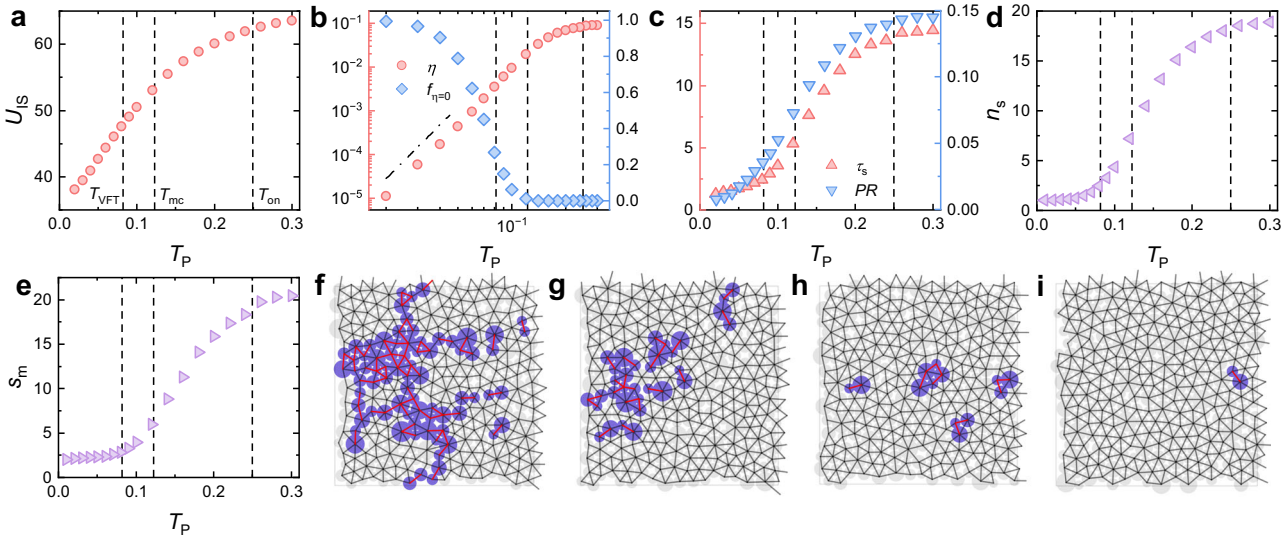

Fig. 7 | Roles of stabilizing bonds in characterizing varying stability from ordinary to ultra-stable glasses. a Energy of inherent structures U_{IS} as a function of parent temperature T_p. **b** Average fraction of stabilizing bonds η and fraction of samples without stabilizing bonds $f_{\eta=0}$ versus T_p. The dot-dashed line indicates $\eta \sim T^4$. **c** Average decay time τ_s of the slowest unstable mode triggered by breaking a stabilizing bond and its corresponding participation ratio (PR) as a function of T_p. **d**, **e** Number n_s and largest size s_m of particle clusters connected via stabilizing bonds versus T_p. Vertical dashed lines in (**a**–**e**) locate characteristic temperatures, T_{VFT}, T_{mc}, and T_{on} (from left to right). Data in (**a**, **b**) are averaged over all samples; data in (**c**–**e**) are averaged only over the $1-f_{\eta=0}$ fraction of samples that contain stabilizing bonds. **f**–**i** Representative configurations of glasses comprising $N = 256$ particles, with bonds quenched from $T_p = 0.300$, 0.140, 0.100, and 0.060, respectively. Stabilizing and non-stabilizing bonds are in red and black, respectively. Particles connected to stabilizing bonds are highlighted in blue. Source data are provided as a Source Data file.

the SI). Therefore, although not derived from vibrational modes, stabilizing bonds still capture key features of QLMs and play a role similar to soft spots. Importantly, stabilizing bonds evolve dynamically in spatial distribution as marginal stability is approached, whereas QLMs and soft spots remain nearly static (Fig. S10 of the SI). This decorrelation signals the onset of marginal stability and underscores the advantage of stabilizing bonds over soft spots in characterizing marginal stability and its mean-field-like nature.

In-depth follow-up studies are required to further verify the role of stabilizing bonds as a new structural order parameter in identifying defective locations in disordered structures by investigating their effects on the mechanical and vibrational properties of disordered solids. Ultra-stable glasses, which contain only isolated stabilizing bonds, are therefore an ideal system to start with. It is interesting to investigate whether these isolated stabilizing bonds could play an analogous role to defects in crystals in influencing the dynamical and vibrational properties of ultra-stable glasses.

Furthermore, we classify jammed solids into two regimes based on their connectivity and stress sensitivity, separated by a crossover pressure p_c. This p_c marks the minimum fraction of stabilizing bonds and signals the loss of isostatic control. Notably, the fractal energy landscape—a key feature of isostatic marginal stability—disappears at a density consistent with our p_c in Weeks-Chandler-Anderson glasses[65,66]. This agreement reinforces our interpretation of p_c via stabilizing bonds. Beyond this crossover, the largely unexplored 'stress-dominant' solids are intriguing. If the rising trend of $\eta(p)$ in Fig. 1a, b persists, all bonds may eventually become stabilizing and equivalent in maintaining stability. This is counterintuitive, as structural heterogeneity typically implies bond inequivalence in disordered solids. What, then, drives these unique characteristics?

Methods

Simulation model

Jammed solids comprise N frictionless particles in an equilateral box of length L. To prevent crystallization, we use a binary mixture of $N/2$ large and $N/2$ small particles with a diameter ratio of 1.4 and equal mass m. Periodic boundary conditions are applied in all directions. Particles interact via a purely repulsive finite-range potential:

$$U(r_{ij}) = \frac{\epsilon}{\alpha}\left(1-\frac{r_{ij}}{d_{ij}}\right)^{\alpha}\Theta\left(1-\frac{r_{ij}}{d_{ij}}\right), \tag{3}$$

where r_{ij} is the distance between particles i and j, d_{ij} is the sum of their radii, ϵ is the energy scale, and $\Theta(x)$ is the Heaviside step function. When $\alpha = 2$ or 2.5, the potential is Harmonic or Hertzian. Units of energy, mass, and length are ϵ, m, and small particle diameter d_s, respectively.

At a given pressure, we generate jammed solids by rapidly quenching high-temperature states to local minima of the enthalpy $H = U + pL^D$ via the fast inertial relaxation engine (FIRE) minimization algorithm[67]. Here, U is the internal energy summed over all interacting particle pairs. We average over 2000 ~ 20000 packings per pressure, depending on system size.

We examine a model glass with particles interacting via an inverse–power–law (IPL) potential:

$$U(r_{ij}) = \left(\frac{d_{ij}}{r_{ij}}\right)^{12} + c_0 + c_2\left(\frac{r_{ij}}{d_{ij}}\right)^2 + c_4\left(\frac{r_{ij}}{d_{ij}}\right)^4, \tag{4}$$

where the interaction is smoothly terminated at $r_{ij} = r_c = 1.25d_{ij}$. The parameters c_0, c_2, and c_4 are selected such that both the potential and its first two derivatives vanish at the cutoff distance, i.e., $U(r_c) = U'(r_c) = U''(r_c) = 0$. The particle diameters d are sampled from the continuous distribution $P(d) = Ad^{-3}$, with A determined by normalization. To enhance glass-forming ability, we employ a non-additive mixing rule for d_{ij} in Eq. (4):

$$d_{ij} = \frac{d_i + d_j}{2}\left(1-\kappa|d_i - d_j|\right), \tag{5}$$

where the parameter κ controls the deviation from additivity; here we set $\kappa = 0.2$ following optimization in previous studies[63]. We set the

average particle diameter $\bar{d}$, mass m, and the Boltzmann constant k_B to be unity. Number density $\rho = N/L^D$ is 1.01 for 2D and 1.0 for 3D systems.

We equilibrate the IPL systems at parent temperature T_p via the swap Monte Carlo algorithm[63]. For the IPL models studied here, the onset, mode-coupling, and Vogel-Fulcher-Tammann temperatures are estimated as: $T_{on} \approx 0.25$ (0.20), $T_{mc} \approx 0.123$ (0.108), and $T_{V\,FT} \approx 0.082$ (0.072) for 2D (3D) systems, respectively[64]. After equilibration, inherent-structural glasses at $T = 0$ are obtained by minimizing the potential energy using the FIRE algorithm[67]. For each T_p, we average over 10000 inherent structures.

To study shear-induced instability, we apply quasistatic shear to the IPL glass by incrementally increasing the shear stress σ, minimizing the enthalpy–like function $\mathcal{H}(R,\gamma) = U - \sigma\gamma L^D$ via the FIRE algorithm[67]. An instability is identified by a sudden change in shear strain γ that occurs at a critical stress $\sigma = \sigma_c$[54]. Lees–Edwards boundary conditions are applied to mimic shear[68].

Normal modes of vibration

Normal modes are obtained by diagonalizing the Hessian matrix:

$$\mathcal{M}(\delta) = \sum_{ij} U''(r_{ij}) \frac{\partial r_{ij}}{\partial \widetilde{\mathbf{R}}} \frac{\partial r_{ij}}{\partial \widetilde{\mathbf{R}}} + \delta \sum_{ij} \frac{U'(r_{ij})}{r_{ij}} \frac{\partial r_{ij}^2}{\partial \widetilde{\mathbf{R}} \partial \widetilde{\mathbf{R}}}, \tag{6}$$

where $\widetilde{\mathbf{R}} = (\mathbf{R}, L)$, $(\mathbf{R}, \gamma)$, and $\mathbf{R}$ for jammed packings at fixed pressure, IPL glasses under shear, and IPL glasses at fixed density, respectively. Here $\mathbf{R} = (\mathbf{r}_1, \mathbf{r}_2, \ldots, \mathbf{r}_N)$ with $\mathbf{r}_i$ $(i = 1, 2, \ldots, N)$ being the location of particle i.

We vary δ to tune the internal stress when calculating $\Delta\eta_\sigma$; otherwise, $\delta = 1$. The same procedure has been used to study the effects of internal stress on jamming transition and vibrational properties of structural glasses[29,69,70].

The participation ratio of a mode is calculated as

$$PR = \frac{(\sum_i |\mathbf{e}_i|^2)^2}{N \sum_i |\mathbf{e}_i|^4}, \tag{7}$$

where $\mathbf{e}_i$ is the polarization vector of particle i in the mode.

Definition of stabilizing bonds

The definition of stabilizing bonds is proposed in Ref. 21. To identify whether a bond is stabilizing or not, we remove it while keeping everything else unchanged. Correspondingly, the Hessian matrix is updated with all terms associated with the bond being removed. If the updated Hessian matrix has a negative eigenvalue, the bond is a stabilizing one. The fraction of stabilizing bonds is the ratio of the number of stabilizing bonds to the total number of bonds.

Data availability

The data that support the findings of this study are included in the article and/or the Supporting Information. The source data underlying the figures are provided with this paper and publicly available on Zenodo at https://doi.org/10.5281/zenodo.20302288[71].

Code availability

The computer codes of this study are available on Zenodo at https://doi.org/10.5281/zenodo.20302288[71].

References

1. Debenedetti, P. G. & Stillinger, F. H. Supercooled liquids and the glass transition. *Nature* **410**, 259 (2001).
2. Cavagna, A. Supercooled liquids for pedestrians. *Phys. Rep.* **476**, 51–124 (2009).
3. Berthier, L. & Biroli, G. Theoretical perspective on the glass transition and amorphous materials. *Rev. Mod. Phys.* **83**, 587 (2011).
4. Charbonneau, P., Kurchan, J., Parisi, G., Urbani, P. & Zamponi, F. Glass and jamming transitions: From exact results to finite-dimensional descriptions. *Annu. Rev. Condens. Matt. Phys.* **8**, 265 (2017).
5. Zallen, R. *The Physics of Amorphous Solids* (John Wiley & Sons, 2008).
6. Berthier, L. & Reichman, D. R. Modern computational studies of the glass transition. *Nat. Rev. Phys.* **5**, 102 (2023).
7. Patinet, S., Vandembroucq, D. & Falk, M. L. Connecting local yield stresses with plastic activity in amorphous solids. *Phys. Rev. Lett.* **117**, 045501 (2016).
8. Tsamados, M., Tanguy, A., Goldenberg, C. & Barrat, J. L. Local elasticity map and plasticity in a model Lennard-Jones glass. *Phys. Rev. E.* **80**, 026112 (2009).
9. Zhang, S. et al. Local and global measures of the shear moduli of jammed disk packings. *Phys. Rev. E.* **107**, 054903 (2023).
10. Richard, D. et al. Predicting plasticity in disordered solids from structural indicators. *Phys. Rev. Mater.* **4**, 113609 (2020).
11. Tong, H. & Tanaka, H. Revealing hidden structural order controlling both fast and slow glassy dynamics in supercooled liquids. *Phys. Rev. X.* **8**, 011041 (2018).
12. Manning, M. L. & Liu, A. J. Vibrational modes identify soft spots in a sheared disordered packing. *Phys. Rev. Lett.* **107**, 108302 (2011).
13. Cubuk, E. D. et al. Structure-property relationships from universal signatures of plasticity in disordered solids. *Science* **358**, 1033–1037 (2017).
14. Tong, H. & Xu, N. Order parameter for structural heterogeneity in disordered solids. *Phys. Rev. E.* **90**, 010401 (2014).
15. Tong, H., Hu, H., Tan, P., Xu, N. & Tanaka, H. Revealing inherent structural characteristics of jammed particulate packings. *Phys. Rev. Lett.* **122**, 215502 (2019).
16. Rissone, P., Corwin, E. I. & & Parisi, G. Long-range anomalous decay of the correlation in jammed packings. *Phys. Rev. Lett.* **127**, 038001 (2021).
17. Goodrich, C. P., Liu, A. J. & Nagel, S. R. The principle of independent bond-level response: Tuning by pruning to exploit disorder for global behavior. *Phys. Rev. Lett.* **114**, 225501 (2015).
18. Huang, J., Zhang, J., Xu, D., Zhang, S., Tong, H. & Xu, N. From jammed solids to mechanical metamaterials: A brief review. *Curr. Opin. Solid State Mater. Sci.* **27**, 101053 (2023).
19. Liu, A. J. & Nagel, S. R. Twenty-five years of the jamming phase diagram. *Nat. Rev. Phys.* **5**, 630–631 (2023).
20. Shen, X. et al. Achieving adjustable elasticity with non-affine to affine transition. *Nat. Mater.* **20**, 1625–1642 (2021).
21. Xu, D., Zhang, S., Liu, A. J., Nagel, S. R. & Xu, N. Discontinuous instabilities in disordered solids. *Proc. Natl Acad. Sci. USA* **120**, e2304974120 (2023).
22. Maxwell, J. C. L. On the calculation of the equilibrium stiffness of frames,. *Philos. Mag.* **27**, 294–299 (1864).
23. van Hecke, M. Jamming of soft particles: geometry, mechanics, scaling and isostaticity. *J. Phys. Condens. Matter* **22**, 033101 (2010).
24. Liu, A. J. & Nagel, S. R. The jamming transition and the marginally jammed solid. *Annu. Rev. Condens. Matt. Phys.* **1**, 347 (2010).
25. Charbonneau, P., Kurchan, J., Parisi, G., Urbani, P. & Zamponi, F. Exact theory of dense amorphous hard spheres in high dimension. III. The full replica symmetry-breaking solution. *J. Stat. Mech.* **10**, P10009 (2014).
26. Charbonneau, P., Kurchan, J., Parisi, G., Urbani, P. & Zamponi, F. Fractal free energy landscapes in structural glasses. *Nat. Commun.* **5**, 3725 (2014).
27. Wyart, M., Silbert, L. E., Nagel, S. R. & Witten, T. A. Effects of compression on the vibrational modes of marginally jammed solids. *Phys. Rev. E.* **72**, 051306 (2005).
28. Wyart, M. Marginal stability constrains force and pair distributions at random close packing. *Phys. Rev. Lett.* **109**, 125502 (2012).

29. DeGiuli, E., Laversanne-Finot, A., Düring, G., Lerner, E. & Wyart, M. Effects of coordination and pressure on sound attenuation, boson peak and elasticity in amorphous solids. *Soft Matter* **10**, 5628 (2014).
30. Lerner, E., Düring, G. & Wyart, M. Low-energy non-linear excitations in sphere packings. *Soft Matter* **9**, 8252–8263 (2013).
31. DeGiuli, E., Lerner, E., Brito, C. & Wyart, M. Force distribution affects vibrational properties in hard-sphere glasses. *Proc. Natl Acad. Sci. USA* **111**, 17054–17059 (2014).
32. Müller, M. & Wyart, M. Marginal stability in structural, spin, and electron glasses. *Annu. Rev. Condens. Matter Phys.* **6**, 177–200 (2015).
33. O'hern, C. S., Silbert, L. E., Liu, A. J. & Nagel, S. R. Jamming at zero temperature and zero applied stress: the epitome of disorder. *Phys. Rev. E.* **68**, 011306 (2003).
34. Parisi, G. & Zamponi, F. Mean-field theory of hard sphere glasses and jamming. *Rev. Mod. Phys.* **82**, 789 (2010).
35. Charbonneau, P., Corwin, E. I., Parisi, G. & Zamponi, F. Jamming criticality revealed by removing localized buckling excitations. *Phys. Rev. Lett.* **114**, 125504 (2015).
36. Xu, N. Mechanical, vibrational, and dynamical properties of amorphous systems near jamming. *Front. Phys.* **6**, 109 (2011).
37. Silbert, L. E., Liu, A. J. & Nagel, S. R. Vibrations and diverging length scales near the unjamming transition. *Phys. Rev. Lett.* **95**, 098301 (2005).
38. Goodrich, C. P., Liu, A. J. & Nagel, S. R. Finite-size scaling at the jamming transition. *Phys. Rev. Lett.* **109**, 095704 (2012).
39. Goodrich, C. P. et al. Jamming in finite systems: stability, anisotropy, fluctuations, and scaling. *Phys. Rev. E.* **90**, 022138 (2014).
40. Zhao, C., Tian, K. & Xu, N. New Jamming scenario: From marginal Jamming to deep Jamming. *Phys. Rev. Lett.* **106**, 125503 (2011).
41. Charbonneau, P., Corwin, E. I., Parisi, G. & Zamponi, F. Universal microstructure and mechanical stability of jammed packings. *Phys. Rev. Lett.* **109**, 205501 (2012).
42. Lerner, E., Düring, G. & Wyart, M. Toward a microscopic description of flow near the jamming threshold. *Europhys. Lett.* **99**, 58003 (2012).
43. Wang, Y., Shang, J., Jin, Y. & Zhang, J. Experimental observations of marginal criticality in granular materials. *Proc. Natl Acad. Sci. USA* **119**, e2204879119 (2022).
44. Ediger, M. D. & Harrowell, P. Perspective: Supercooled liquids and glasses. *J. Chem. Phys.* **137**, 080901 (2012).
45. Lubchenko, V. & Wolynes, P. G. Theory of structural glasses and supercooled liquids. *Annu. Rev. Phys. Chem.* **58**, 235–266 (2007).
46. Swallen, S. F. et al. Organic glasses with exceptional thermodynamic and kinetic stability. *Science* **315**, 353–356 (2007).
47. Berthier, L., Coslovich, D., Ninarello, A. & Ozawa, M. Equilibrium sampling of hard spheres up to the Jamming density and beyond. *Phys. Rev. Lett.* **116**, 238002 (2016).
48. Ozawa, M., Iwashita, Y., Kob, W. & Zamponi, F. Creating bulk ultrastable glasses by random particle bonding. *Nat. Commun.* **14**, 113 (2023).
49. Bu, H. et al. Accessing ultrastable glass via a bulk transformation. *Nat. Commun.* **16**, 562 (2025).
50. Leoni, F., Russo, J., Sciortino, F. & Yanagishima, T. Generating ultrastable glasses by homogenizing the local virial stress. *Phys. Rev. Lett.* **134**, 128201 (2025).
51. Maloney, C. E. & Lemaître, A. Subextensive scaling in the athermal, quasistatic limit of amorphous matter in plastic shear flow. *Phys. Rev. Lett.* **93**, 016001 (2004).
52. Maloney, C. E. & Lemaître, A. Universal breakdown of elasticity at the onset of material failure. *Phys. Rev. Lett.* **93**, 195501 (2004).
53. Lacks, D. J. Localized mechanical instabilities and structural transformations in silica glass under high pressure. *Phys. Rev. Lett.* **80**, 5385 (1998).
54. Xu, N., Liu, A. J. & Nagel, S. R. Instabilities of jammed packings of frictionless spheres under load. *Phys. Rev. Lett.* **119**, 215502 (2017).
55. Shang, J., Wang, Y., Pan, D., Jin, Y. & Zhang, J. The yielding of granular matter is marginally stable and critical. *Proc. Natl. Acad. Sci. USA* **121**, e2402843121 (2024).
56. Matsushima, T. & Blumenfeld, R. Universal structural characteristics of planar granular packs. *Phys. Rev. Lett.* **112**, 098003 (2014).
57. Liu, H., Xie, X. & Xu, N. Finite size analysis of zero-temperature jamming transition under applied shear stress by minimizing a thermodynamic-like potential. *Phys. Rev. Lett.* **112**, 145502 (2014).
58. Wang, X., Zheng, W., Wang, L. & Xu, N. Disordered solids without well-defined transverse phonons: The nature of hard sphere glasses. *Phys. Rev. Lett.* **114**, 035502 (2015).
59. Oyama, N., Mizuno, H. & Ikeda, A. Shear-induced criticality in glasses shares qualitative similarities with the Gardner phase. *Soft Matter* **19**, 6074 (2023).
60. Oyama, N., Mizuno, H. & Ikeda, A. Unified view of avalanche criticality in sheared glasses. *Phys. Rev. E* **104**, 015002 (2021).
61. Ozawa, M., Berthier, L., Biroli, G., Rosso, A. & Tarjus, G. Random critical point separates brittle and ductile yielding transitions in amorphous materials. *Proc. Natl Acad. Sci. USA* **115**, 6656–6661 (2018).
62. Divoux, T. et al. Ductile-to-brittle transition and yielding in soft amorphous materials: perspectives and open questions. *Soft Matter* **20**, 6868–6888 (2024).
63. Ninarello, A., Berthier, L. & Coslovich, D. Models and algorithms for the next generation of glass transition studies. *Phys. Rev. X.* **7**, 021039 (2017).
64. Berthier, L., Charbonneau, P., Ninarello, A., Ozawa, M. & Yaida, S. Zero-temperature glass transition in two dimensions. *Nat. Commun.* **10**, 1508 (2019).
65. Scalliet, C. & Berthier, L. Rejuvenation and memory effects in a structural glass. *Phys. Rev. Lett.* **122**, 255502 (2019).
66. Scalliet, C., Berthier, L. & Zamponi, F. Nature of excitations and defects in structural glasses. *Nat. Commun.* **10**, 5102 (2019).
67. Bitzek, E., Koskinen, P., Gähler, F., Moseler, M. & Gumbsch, P. Structural relaxation made simple. *Phys. Rev. Lett.* **97**, 170201 (2006).
68. Allen, M. P. & Tildesley, D. J. *Computer Simulation of Liquids* (Oxford University Press, 1989).
69. Xu, N., Vitelli, V., Liu, A. J. & Nagel, S. R. Anharmonic and quasi-localized vibrations in jammed solids—Modes for mechanical failure. *Europhys. Lett.* **90**, 56001 (2010).
70. Lerner, E. & Bouchbinder, E. Frustration-induced internal stresses are responsible for quasilocalized modes in structural glasses. *Phys. Rev. E.* **97**, 032140 (2018).
71. Huang, J. et al. Revealing bond level origin of stability in disordered solids from marginal stability to ultrastability. *Zenodo*. Dataset. https://doi.org/10.5281/zenodo.20302288 (2026).

Acknowledgements

We are grateful to Andrea J. Liu for insightful discussions. We also thank the Supercomputing Center of the University of Science and Technology of China for the computer time.

Author contributions

N.X. designed the project. N.X. and H.T. supervised the project. J.H. performed the simulations. J.H., J.Z., D.X., S.Z., H.T. and N.X. analyzed the data. J.H., H.T. and N.X. wrote the paper.

Funding

This work was supported by the National Natural Science Foundation of China Grant Nos. 12334009 (N.X. and H.T.) and 12274392 (H.T.), Fundamental and Interdisciplinary Disciplines Breakthrough Plan of the Ministry of Education of China No. JYB2025XDXM502 (N.X.), and Guizhou Provincial Major Scientific and Technological Program XKBF(2025)010 (N.X.).

Competing interests
The authors declare no competing interests.

Additional information
Supplementary information The online version contains supplementary material available at https://doi.org/10.1038/s41467-026-73939-8.

Correspondence and requests for materials should be addressed to Hua Tong or Ning Xu.

Peer review information *Nature Communications* thanks Misaki Ozawa, and the other, anonymous, reviewers for their contribution to the peer review of this work. A peer review file is available.